SeCap: Self-Calibrating and Adaptive Prompts for Cross-view Person Re-Identification in Aerial-Ground Networks

Shining Wang[1,2,4*], Yunlong Wang[1,2,4*], Ruiqi Wu[1,2,4], Bingliang Jiao[1,2,4], Wenxuan Wang[1,3,4†], Peng Wang[1,2,4]

[1]School of Computer Science, Northwestern Polytechnical University, China.
[2]Ningbo Institute, Northwestern Polytechnical University, China.
[3]Shenzhen Research Institute, Northwestern Polytechnical University, China.
[4]National Engineering Laboratory for integrated Aero-Space-Ground-Ocean, Xi'an, Shaanxi, China.

{wangshining, wangyunlong2019, wurq, bingliang.jiao}@mail.nwpu.edu.cn {wxwang, peng.wang}@nwpu.edu.cn

Abstract

When discussing the Aerial-Ground Person Re-identification (AGPReID) task, we face the main challenge of the significant appearance variations caused by different viewpoints, making identity matching difficult. To address this issue, previous methods attempt to reduce the differences between viewpoints by critical attributes and decoupling the viewpoints. While these methods can mitigate viewpoint differences to some extent, they still face two main issues: (1) difficulty in handling viewpoint diversity and (2) neglect of the contribution of local features. To effectively address these challenges, we design and implement the Self-Calibrating and Adaptive Prompt (SeCap) method for the AGPReID task. The core of this framework relies on the Prompt Re-calibration Module (PRM), which adaptively re-calibrates prompts based on the input. Combined with the Local Feature Refinement Module (LFRM), SeCap can extract view-invariant features from local features for AGPReID. Meanwhile, given the current scarcity of datasets in the AGPReID field, we further contribute two real-world Large-scale Aerial-Ground Person Re-Identification datasets, LAGPeR and G2APS-ReID. The former is collected and annotated by us independently, covering 4,231 unique identities and containing 63,841 high-quality images; the latter is reconstructed from the person search dataset G2APS. Through extensive experiments on AGPReID datasets, we demonstrate that SeCap is a feasible and effective solution for the AGPReID task. The datasets and source code available on https://github.com/wangshining681/SeCap-AGPReID.
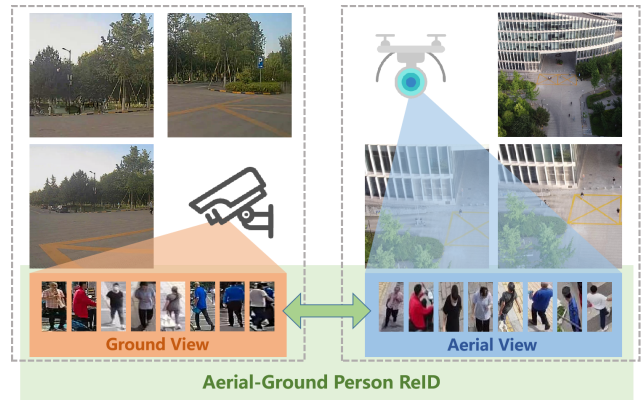
Figure 1. Aerial View and Ground View exhibit significant appearance variation due to notable differences in views. This variation poses substantial challenges for cross-view image matching.

1. Introduction

Person re-identification (ReID), as the cornerstone of intelligent surveillance systems, fundamentally relies on accurately identifying individuals across different camera viewpoints and complex environmental changes [11, 12, 23, 25, 29, 37]. However, traditional ReID methods are often limited to the same view, such as ground view [24, 27, 34–36, 41] or aerial view [4, 10, 14, 28, 39], and fail to adequately address the challenges posed by extreme visual transformations and the integration of complementary information in cross-view scenarios (e.g., combining ground and aerial cameras). These challenges are more prevalent in real-world applications, thereby introducing the problem of the Aerial-Ground Person Re-Identification (AGPReID).

As shown in Fig. 1, unlike traditional ReID tasks, the query and gallery sets in AGPReID are captured separately by aerial-view or ground-view cameras [20, 21, 38], respectively. This results in significant variations in the compared

---

Table 1. Statistical comparisons with existing datasets, including view-homogeneous (ground or aerial) and view-heterogeneous (ground and aerial) ReID.

DATASET	VIEW	SOURCE	#IDENTITY	#CAMERA	#IMAGE	HEIGHT
Market1501 [42]	Ground	Real	1,501	16	32,668	<10m
DukeMTMC-reID [43]	Ground	Real	1,404	8	36,411	<10m
PRAI1581 [39]	Aerial	Real	1,581	2	39,461	20~60m
UAVHuman [14]	Aerial	Real	1,144	1	41,290	2-8m
AG-ReID.v1 [20]	Aerial-Ground	Real	388	2(1A+1G)	21,893	15~45m
AG-ReID.v2 [21]	Aerial-Ground-Wearable	Real	1,615	3(1A+1G+1W)	100,502	15~45m
CARGO [38]	Aerial-Ground	Synthetic	5,000	13(5A+8G)	108,563	5~75m
G2APS-ReID(Ours)	**Aerial-Ground**	**Real**	**2,788**	**2(1A+1G)**	**200,864**	**20~60m**
LAGPeR(Ours)	**Aerial-Ground**	**Real**	**4,231**	**21(7A+14G)**	**63,841**	**20~60m**

person images, making identity matching more challenging [15, 32]. To address this issue, AG-ReID [20, 21] utilizes identity attributes to extract view-invariant information, partially solving the cross-view matching problem. Additionally, VDT [38] designs the view decoupling transformer based on ViT [16], using a hierarchical decoupling mechanism to extract view-invariant features effectively.

Although existing methods can partially solve the cross-view matching problem, they still suffer from over-reliance on attributes, insufficient adaptation to multiple views, etc. Specifically, there are two main issues with current methods: (1) *Difficulty in Handling Viewpoint Diversity*: In AGPReID tasks, the variability of viewpoints renders decoupling methods within a single viewpoint insufficient for all viewpoints. (2) *Neglect of Local Features*: Due to the steep downward viewing angles of drones, various parts of the body are often not fully exposed in the images, especially when person are occluded [7, 18, 22, 27]. AG-ReID [20] extracts cross-view information by attributes, which essentially rely on view-invariant local features. However, the attribute labels hinder generalization. Therefore, we must consider learning view-invariant local features from different viewpoints without dependency on labels.

To overcome these challenges, this paper proposes an AGPReID framework named SeCap, which self-calibrates and adaptively generates prompts based on the inputs for cross-view person re-identification. This framework adopts an encoder-decoder transformer architecture. The encoder employs the View Decoupling Transformer (VDT) for viewpoint decoupling, while the decoder further decodes local features using the view-invariant features. Specifically, the decoder comprises the Prompt Re-calibration Module (PRM) and the Local Feature Refinement Module (LPRM). To address the challenge of viewpoint diversity (limitation 1), we design the PRM to re-calibrate prompts based on the input adaptively. It dynamically generates and self-calibrates prompts that closely align with the current view-

point, thus adapt to different viewpoints. To fully leverage the role of local features (limitation 2), we design the LPRM for local feature refinement. This module uses recalibrated prompts and employs the to-way attention mechanism to synchronously update various features, thereby learning view-invariant information from local features.

Furthermore, as shown in Tab. 1, due to the scarcity of datasets for the AGPReID task, we contribute two real-world large-scale aerial-ground person re-identification datasets, LAGPeR and G2APS-ReID. The LAGPeR dataset, which is independently collected, annotated, and partitioned by us, is gathered from campus scenes using a combination of seven drone cameras and fourteen ground cameras, capturing a total of $4,231$ unique identities across $63,841$ images. This dataset fully considers the impacts of occlusion, lighting, and cross-domain variations that may be encountered in real-world applications. To further expand the AGPReID dataset, we also reconstruct the G2APS-ReID from the person search dataset G2APS [40]. For the comprehensive evaluation of various AGPReID methods, we meticulously design the evaluation settings that account for the retrieval demands across both ground and aerial viewpoints, thereby thoroughly evaluating the models' effectiveness in handling cross-view re-identification tasks. In summary, the main contributions of this paper include:

- Introducing an innovative AGPReID method called SeCap, adaptively re-calibrate prompts to match the current view based on the input, significantly enhancing the AGPReID performance.
- Contribute two real-world large-scale AGPReID datasets, LAGPeR and G2APS-ReID, which provide significant data support for research in the AGPReID task.
- Conduct extensive experiments on AGPReID datasets, demonstrating our SeCap's superiority in AGPReID tasks and achieving state-of-the-art (SOTA) performance.

2. Related Work

2.1. View-Invariant Person Re-Identification

Research on view-invariant ReID typically focuses on two main categories: ground-view [3, 9, 42, 43] and aerial-view perspectives [4, 14, 39]. Existing studies contribute a plethora of ground-view datasets, such as Market1501 [42] and MSMT17 [30], which significantly advance the field. In recent years, with the maturation and widespread application of Transformer architectures, Vision Transformer (ViT) models [16] gradually emerged in the ReID domain [7], become the mainstream backbone for feature extraction. Against this backdrop, as an emerging technological paradigm, prompt learning is widely applied in various ReID tasks [8, 13], demonstrating its ability to retain the inherent knowledge of the backbone model while adapting it to various tasks [8, 26, 31, 33]. This inspires us to use prompt learning to solve the AGPReID problem. Overall, compared to view-invariant ReID, research on cross-view ReID is relatively sparse, especially concerning the significant appearance changes caused by aerial and ground-view variations. Therefore, our work focuses on the aerial-ground cross-view person ReID task, aiming to find an effective method to address this challenge.

2.2. Aerial-Ground Cross-View ReID

The core challenge of the aerial-ground person re-identification (AGPReID) lies in the significant appearance variations caused by different viewpoints, making identity matching difficult. To address this challenge, AG-ReID [20] solves the cross-view matching problem by leveraging identity attributes, making individuals with similar attributes more likely to be identified as the same person. Meanwhile, AG-ReIDv2 [21] introduces the Elevated-View Attention Stream to fully utilize the invariant local information between ground and aerial view for identity discrimination, which also demonstrates the importance of local features in AGPReID tasks. However, these two works rely on attributes and do not consider the decoupling of view-invariant information within local features, limiting the scalability of the method. Another approach aligns feature spaces from different viewpoints, as in VDT [38], which designs the view-decoupling transformer based on ViT [16], effectively extracting view-invariant features through a hierarchical decoupling mechanism. Although this method can partially decouple view-related information, the diversity of viewpoints in AGPReID may lead to over-separation of potentially useful information within view-invariant features, and even result in the loss of inherent knowledge of the backbone network. Different from existing works, our proposed framework, SeCap, can adaptively adjust prompts based on inputs to generate prompts suitable for different viewpoints, effectively separating view-invariant features.

2.3. Aerial-Ground ReID Datasets

In the AGPReID field, the scarcity and limitations of datasets become the key factors constraining research progress. Compared to mature view-invariant datasets [42, 43], AGPReID datasets are scarce in number and far from meeting research needs in terms of real-world data scale. For instance, the number of identity IDs in AG-ReID.v1 [20] datasets is far lower than in-ground ReID datasets like Market1501 [42] and DukeMTMC-reID [43], highlighting the lack of data resources in this field. Although AG-ReID.v2 [21] attempts to address this shortfall by expanding the dataset, the large number of wearable device images included in the new data does not substantially enhance coverage of the differences between aerial and ground views, affecting its practical value. Additionally, synthetic datasets like CARGO [38], while approaching real datasets in scale, lack real-world complexity, limiting model performance in actual scenarios. Therefore, developing the larger-scale aerial-ground cross-view ReID dataset, and designing efficient algorithms to utilize these datasets effectively, become urgent problems to be solved in this field. To overcome this problem, we contribute two real-world large-scale AGPReID datasets: LAGPeR and G2APS-ReID.

3. Method

3.1. Overview

The overall framework of SeCap, as illustrated in Fig. 2 (a), adopts an encoder-decoder transformer architecture. The encoder is the view decoupling transformer (VDT) [38]. In contrast to the conventional ViT [16], our approach incorporates the **View** token and performs hierarchical decoupling of the **Cls** token at each layer, effectively segregating view-related and view-invariant features within the **Cls** token, while extracting local features from the input. The decoder comprises the Prompt Re-calibration Module (**PRM**) and the Local Feature Refinement Module (**LFRM**). The **PRM** adaptively generates and re-calibrates prompts for different viewpoints based on the current viewpoint information. Concurrently, the **LFRM** utilizes the re-calibrated prompts from the **PRM** to decode the local features. The overall framework can be described as follows:

$$[\mathbf{Cls}, \mathbf{View}, X_{\text{local}}] = \text{VDT}([\mathbf{CLS}, \mathbf{View}, [\text{tokenization}(\mathbf{X})]])$$
$$X_{\text{inv}} = \mathbf{Cls} - \mathbf{View}$$
$$X_{\text{local}} = \mathbf{LFRM}(X_{\text{local}}, \mathbf{PRM}(\mathbf{Prompt}, X_{\text{inv}}))$$
$$\mathbf{Out} = [X_{\text{inv}}, X_{\text{local}}]$$
$$(1)$$

where VDT is the View Decoupling Transformer, **Cls** and **View** are the Class and View token, tokenization($\mathbf{X}$) refers to the process of converting the inputs $\mathbf{X}$ into tokens, X_{inv} represents the view-invariant features, **Prompt** denotes learnable prompts, X_{local} signifies the local features of the
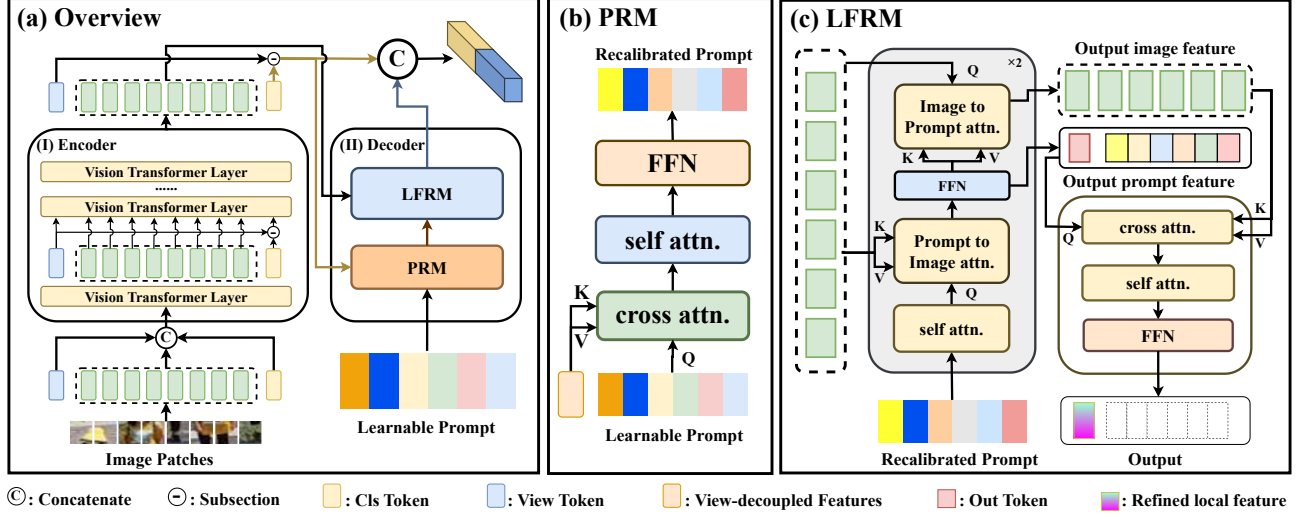
Figure 2. (a) The architecture of the proposed SeCap. The key component is an encoder-decoder transformer. The encoder extracts the visual features of the picture and decouples the viewpoints. The decoder re-calibrates prompts through the current viewpoint information and decodes the local features using the re-calibrated prompts. (b) The Prompt Re-calibration Module (PRM) adaptively generates and re-calibrates prompts for different viewpoints according to view-invariant features. (c) The Local Feature Refinement Module (LFRM) finely decodes discriminative features from the local features using the re-calibrated prompts in PRM.

input data, and **Out** is the final output.

3.2. Prompt Re-calibration Module

The Prompt Re-calibration Module (**PRM**) is designed based on the Transformer Decoder architecture [2], aiming at adaptively re-calibrating prompts suitable for different viewpoints. Specifically, this module initializes and maintains a set of prompts with learnable vectors **Prompt** = $[\text{Prompt}_1, \text{Prompt}_2, \dots, \text{Prompt}_L]$, where **L** is the hyperparameter that denotes the prompt length.

As illustrated in Fig. 2 (b), the module initially incorporates the view-invariant features into prompts via cross-attention, enhancing prompts' focus on view-invariant information within visual features. Subsequently, the self-attention mechanism is employed to amalgamate and re-calibrate the information of each prompt within the prompts sequence, ensuring comprehensive integration of the view-invariant information. Finally, the Feed-Forward Network (FFN) is applied to produce the re-calibrated prompts tailored to the view-invariant information. The Prompt Re-calibration Module can be described as follows:

$$P_{re} = \text{FFN}(\text{SA}(\text{CA}(\textbf{Prompt}, X_{inv}, X_{inv}))) + \textbf{Prompt} \quad (2)$$

where X_{inv} represents the view-invariant features extracted from the backbone, **Prompt** denotes learnable prompts, CA is the cross-attention mechanism that aligns prompts with the view-invariant features, SA is the self-attention mechanism that enables the model to weigh the importance of different parts of the input, FFN stands for the Feed-Forward Network, and P_{re} is the re-calibrated prompts.

3.3. Local Feature Refinement Module

The Local Feature Refinement Module (**LFRM**) is the Transformer-based decoder, as illustrated in Fig 2 (c). It extracts the view-invariant features of the local features F_{local}, using the re-calibrated prompts P_{re} from the **PRM**. The re-calibrated prompts integrate view-invariant information from the global features, enabling the **LFRM** to decode view-invariant features of the local features, thereby aligning the local features with the global features.

Specifically, the **LFRM** consists of the two-way attention module and the feature fusion module. The two-way attention module employs both self-attention and cross-attention mechanisms in both prompt-to-image encoding and image-to-prompt encoding directions, to dynamically update and enhance all feature representations. Through the two-way attention module, the **LFRM** efficiently integrates and updates the visual information of the local features and view-invariant information of the re-calibrated prompts. The two-way attention module can be described as follows:

$$\begin{aligned} F_P &= \text{FFN}(\text{CA}(\text{SA}(P_{re}), F_{local}, F_{local})) + P_{re} \\ F_I &= \text{CA}(F_{local}, F_P, F_P) + F_{local} \end{aligned} \quad (3)$$

where F_P represents the prompt features output by the two-way attention module, F_I denotes the image features output by the two-way attention module, FFN stands for the Feed-Forward Network, CA is the cross-attention mechanism, SA

is the self-attention mechanism, F_{local} signifies the local features, and P_{re} refers to the re-calibrated prompts.

To maintain the light weight of the decoder, we only stack two two-way attention blocks in **LFRM**. Additionally, the feature fusion module employs cross-attention and self-attention to further integrate the image features and prompt features output by the two-way attention module, thereby decoding view-invariant features of the local features. The feature fusion module can be described as follows:

$$[\textbf{Out}, \_] = \text{FFN}(\text{SA}(\text{CA}([\textbf{Out}, F_P], F_I, F_I))) \quad (4)$$

where **Out** is output token, which integrates the final output, F_P is the prompt features, F_I is the image features.

3.4. Optimization

In addition to the commonly employ the ID classification loss and the Triplet loss in ReID tasks, the loss functions in our model are further enhanced with the view classification loss and the orthogonality loss.

View Classification Loss: To achieve the decoupling of view-related features, we utilize a view classifier to guide the extraction of view-related features and employ the view classification loss for constraint. The loss function for this process can be formalized as follows:

$$\mathcal{L}_{\text{view}} = -\sum_{i=1}^{N} y_i \log(p_i) \quad (5)$$

where y_i is the ground truth label of view for the i-th sample, indicating the actual view class, p_i is the predicted probability of the i-th sample belonging to the correct view class, and N is the total number of samples in the dataset.

Orthogonality Loss: To quantify the effectiveness of view decoupling, we introduce the orthogonality loss to ensure thorough decoupling. The specific expression of the orthogonality loss is as follows:

$$\mathcal{L}_{\text{orth}} = \sum_{i=1}^{d} |\langle \textbf{inv}_i, \textbf{v}_i \rangle| \quad (6)$$

where $|\langle \cdot, \cdot \rangle|$ denotes the absolute value of the dot product between two features, which is used to measure their linear correlation. d represents the dimensionality of the features. $\textbf{inv}_i$ and $\textbf{v}_i$ refer to the i-th dimension of the view-invariant and view-related features.

Overall Loss: We apply the ID classification loss and the Triplet loss to the global and local features to guide the model's learning. Due to the significant difference in the number of categories between the view classifier and the ID classifier (in the thousands), the view classification loss is scaled by a small coefficient λ to balance the difficulty between view and ID classification. The impact of this coefficient is analyzed in **Supplementary Material**. The overall

optimization objective can be summarized as follows:

$$\begin{aligned}
\mathcal{L} = {} & \alpha(\mathcal{L}_{ID}^{global} + \mathcal{L}_{Tri}^{global}) \\
& + \beta(\mathcal{L}_{ID}^{local} + \mathcal{L}_{Tri}^{local}) \\
& + \lambda(\mathcal{L}_v + \mathcal{L}_\rho),
\end{aligned} \quad (7)$$

where λ is the hyperparameter used to balance the different difficulties of view classification and ID classification, α and β are also the hyperparameter to balance the optimization objectives of global and local features.

4. Datasets

To expand the datasets available for the AGPReID task, we contribute the **LAGPeR** and **G2APS-ReID** datasets as shown in Tab. 1. The LAGPeR dataset is independently collected, annotated, and partitioned by us, and it includes data from **21 cameras**, **7 scenes**, and **3 perspectives** (with ground perspectives divided into oblique and frontal views). For detailed information on data collection, annotation, partitioning, and experimental setup, please refer to Sec. 4.1. The G2APS-ReID dataset is reconstructed from the large-scale person search dataset G2APS [40]. Since the original G2APS dataset only considers retrieval tasks from ground to aerial view, which do not fully meet the requirements of the AGPReID task, we re-partition the G2APS. Detailed procedures are elaborated in Sec. 4.2.

4.1. LAGPeR

Data Collection: Our image data is obtained using fixed Hikvision and DJI drone cameras, capturing video footage from 14 fixed and 7 drone cameras. The dataset encompasses $4,231$ pedestrians, totaling $63,841$ images. The drone's video footage is taken from heights ranging between 20 to 60 meters. The data collection process spans approximately two months and includes various scenes(teaching area, supermarket, canteen, etc.), lighting conditions(such as day or night), weather conditions (sunny or rainy), and viewing angles (straight-ahead angle, oblique angle, or high angle).

Data Annotation: All our datasets are manually annotated by human annotators. The image data is sampled from the collected video footage. Fixed cameras sample one frame every 10 frames, while drone cameras sample one frame every 24 frames. The naming convention for person images is 000X_C0Y_00000Z.jpg, where 000X denotes the person ID, C0Y indicates the camera ID, and 00000Z represents the frame position in the corresponding video. The cropped images are 128×256 pixels in size.

Data Division and Experimental Setup: For the LAGPeR dataset, we select 12 cameras (including 8 ground cameras and 4 drone cameras) from the first four scenes as the training set, while images from 9 cameras in the remaining three scenes are used for evaluation. To simulate

Table 2. Experimental setup and data division of the LAGPeR and G2APS-ReID datasets.

SETTING	SUBSET	#View.	LAGPeR			G2APS-ReID		
			#Cam	#IDs	#Images	#Cam	#IDs	#Images
-	Train	Aerial+Ground	12	2,708	40,770	2	1,569	100,871
$A \rightarrow G$	Query	Aerial	3	1,523	3,046	1	1,219	4,876
	Gallery	Ground	6	1,523	15,533	1	1,219	37,202
$G \rightarrow A$	Query	Ground	6	1,523	3,046	1	1,219	4,876
	Gallery	Aerial	3	1,523	7,717	1	1,219	62,791
$G \rightarrow A + G$	Query	Ground	6	1,523	3,046	-	-	-
	Gallery	Aerial+Ground	9	1,523	20,204	-	-	-

real-world disturbances, we include IDs that appear only in one camera as noise items in the dataset. After filtering, we identify $1,523$ IDs for evaluation, while the remaining $2,708$ IDs are used as the training set. During the data prepossessing stage, we aim to select the most representative images for each ID as query images. To achieve this, we employ a method based on gradient histograms and K-nearest neighbor clustering algorithms. Ultimately, we successfully select $3,046$ images of $1,523$ IDs from each perspective as query images, constructing a comprehensive task setup (as shown in Tab. 2). In terms of the experimental setup, compared to conventional AGPReID datasets, we add $G \rightarrow A + G$ setting, which includes images from both ground and aerial viewpoints in the gallery to evaluate the model's performance more comprehensively.

4.2. G2APS-ReID

Reconstruction and Experimental Setup: The original G2APS [40] dataset primarily focuses on ground-to-aerial retrieval and has limitations on the single evaluation perspective for the Person Search. Therefore, we reconstruct the G2APS to create the G2APS-ReID dataset. Specifically, we randomly select 60% of the IDs as the training set and the remaining as the test set. We manually adjust the IDs in the test set by reallocating IDs with too few or too many images to the training set, resulting in $1,219$ IDs for evaluation and $1,509$ IDs for training. Regarding the experimental setup, since each ID in the G2APS [40] dataset includes only two cameras (one ground and one aerial), cross-camera retrieval cannot be performed from a ground perspective. Therefore, we do not include the $G \rightarrow A + G$ setting.

5. Experiments

5.1. Experimental Settings

Dataset. We evaluate SeCap using five AGPReID datasets, including the existing AG-ReID.v1 [20], AG-ReID.v2 [21], CARGO [38], and our proposed LAGPeR and G2APS-ReID. The results of AG-ReID.v2 and CARGO are pre-

sented in the supplementary material.
(1) LAGPeR: The dataset includes $4,231$ IDs and $63,841$ images, collected from 21 cameras. Among these, samples from $2,708$ IDs are used for training, while images from the remaining $1,523$ IDs constitute the test set. The test set is divided into three experimental setups: $A \rightarrow G$, $G \rightarrow A$, and $G \rightarrow A + G$, with specific divisions detailed in Tab. 2. To better evaluate the model's robustness against interference, we additionally include images with incorrectly labeled IDs as noise items in the gallery. These images only appear under a single camera, and are marked as -1.
(2) G2APS-ReID The dataset contains $200,864$ images from $2,788$ IDs, captured by two types of cameras: ground and aerial. Of these, samples from $1,509$ IDs are used for training, while samples from the remaining $1,219$ IDs are designated for testing. The test set includes two experimental setups: $A \rightarrow G$ and $G \rightarrow A$. We also include the data that appears under a single view as noise items in the gallery. Since there is only one ground camera, we do not include the $G \rightarrow A + G$ experimental setting.
(3) AG-ReID.v1: The dataset comprises $21,893$ images with 388 IDs, captured by two cameras: ground and aerial. Of these, 199 IDs are designated for the training set, while the remaining 189 IDs are used for the test set. The dataset also includes 15 attributes to aid in cross-view matching. In terms of experimental setup, the test images are evaluated under two experimental settings: $A \rightarrow G$ and $G \rightarrow A$.
Metric. To comprehensively evaluate SeCap, we adopt Rank-1 cumulative matching characteristics and mean Average Precision (mAP) as evaluation metrics. These metrics quantitatively assess the model's retrieval capability from both accuracy and recall, providing strong support for subsequent model optimization and comparative analysis.
Implementation Details. Our method is implemented on the PyTorch and utilizes one NVIDIA RTX 3090 GPU for all experiments. Our model employs the Vision Transformer [16], pre-trained on ImageNet [5] as the backbone model. During inference and training, the inputs are resized to 256×128. In the tokenization process, the patch and

Table 3. Performance comparison on LAGPeR and G2APS-ReID datasets. '$A \rightarrow G$' denotes that the Aerial view is the query, '$G \rightarrow A$' denotes that the Ground view is the query, and '$G \rightarrow A + G$' indicates that the gallery contains images from both the Aerial and Ground view. CLIP-ReID[*] indicates using OLP and SIE in Clip-ReID. MIP[†] represents the re-implementation for the AGPReID. AG-ReID[‡] indicates removing the attributes branch of the AG-ReID method. The best performance is in **bold**.

| METHOD | BACKBONE | LAGPeR | | | | | | G2APS-ReID | | | |
| | | $A \rightarrow G$ | | $G \rightarrow A$ | | $G \rightarrow A + G$ | | $A \rightarrow G$ | | $G \rightarrow A$ | |
		Rank-1	mAP	Rank-1	mAP	Rank-1	mAP	Rank-1	mAP	Rank-1	mAP
ViT [17]	ViT	38.67	27.25	32.04	30.69	18.88	15.31	69.38	52.17	67.16	52.22
TransReID [7]	ViT	38.80	28.80	33.00	32.10	22.90	18.80	67.10	53.10	68.52	54.19
CLIP-ReID [13]	CLIP	24.40	17.60	21.30	20.80	12.30	10.20	58.30	42.20	56.41	41.92
CLIP-ReID[*] [13]	CLIP	23.10	17.50	20.00	20.30	9.00	8.40	59.60	42.70	56.39	42.52
MIP[†] [31]	ViT	39.30	29.30	33.90	32.60	21.00	17.30	73.00	57.40	70.22	57.06
AG-ReID[‡] [20]	ViT	40.48	28.89	32.96	31.91	22.03	17.89	70.75	52.87	68.70	53.39
VDT [38]	ViT	40.15	28.97	33.55	31.98	19.50	16.45	73.05	56.23	71.08	56.01
SeCap(Ours)	ViT	**41.79**	**30.37**	**35.26**	**33.42**	**24.39**	**19.24**	**75.31**	**58.57**	**73.22**	**58.90**

Table 4. Performance comparison under two settings of AG-ReID.v1 dataset. '$A \rightarrow G$' and '$G \rightarrow A$' represent the performance in two cross-view settings. 'BB' refers to the backbone. CLIP-ReID[*] indicates using OLP and SIE in Clip-ReID. The best performance is in **bold**.

| METHOD | BB | $A \rightarrow G$ | | $G \rightarrow A$ | |
		Rank-1	mAP	Rank-1	mAP
CLIP-ReID [13]	CLIP	72.61	62.09	74.12	64.19
CLIP-ReID[*] [13]	CLIP	74.81	64.18	74.82	66.11
ViT [17]	ViT	78.81	69.18	81.61	73.03
AG-ReID [20]	ViT	81.47	72.38	82.85	73.35
VDT [38]	ViT	82.91	74.44	86.59	**78.57**
SeCap(Ours)	ViT	**84.03**	**76.16**	**87.01**	78.34

stride sizes are set to 16×16, and the embedding shape d of tokens is set to 768. Data augmentation is applied to transform the images during training, including random cropping, color jittering, random erasing, etc. The batch size is 64, comprising 16 identities with 4 images per identity. We adopt the soft version of triplet loss [34] to avoid manual selection of m in the triplet loss formulation. The model is trained 120 epochs using the Stochastic Gradient Descent (SGD) [19] optimizer. A cosine learning rate decay schedule is utilized, reducing the learning rate from 8×10^{-3} to a final value of 1.6×10^{-6}. During inference, no data augmentation or re-ranking techniques are applied.

5.2. Performance of SeCap

As shown in Tab. 3 and Tab. 4, for evaluation fairness, we focus exclusively on Transformer-based architectures (particularly ViT [16]). Specifically, we compare the single-

view ReID methods ViT [17], Clip-ReID [13], and TransReID [7], all using ViT as the backbone (the image encoder of CLIP-ReID uses the ViT-based method). We also compare AGPReID methods, including AG-ReID [20] and VDT [38], as well as the cross-modal ReID method MIP [31], re-implemented for AGPReID.

Our SeCap method can achieve state-of-the-art (SOTA) performance on the LAGPeR and G2APS-ReID datasets. Compared to the baseline method (ViT), our SeCap demonstrates significant performance improvements. Our approach outperforms all competitors across five configurations in two datasets, especially showing notable enhancements in cross-view matching tasks. In comparison to cross-view methods, our approach consistently surpasses AG-ReID [20] and VDT [38] across various cross-view tasks. Notably, in the $G \rightarrow A + G$ setting, which tests the model's comprehensive performance, our method significantly outperforms other cross-view methods. Furthermore, on the AG-ReID.v1 dataset, even though our method does not use the attributes provided by the AG-ReID.v1 dataset, we still achieve the best results in the '$A \rightarrow G$' setting, and comparable results for the '$G \rightarrow A$' setting. These remarkable results show our Secap can learn better view-invariant features to boost model performance.

Compared to single-view competitors, our method demonstrates significant improvements in the cross-view settings of LAGPeR and G2APS-ReID, surpassing the Vision Transformer (ViT) by 3% on LAGPeR and 6% on G2APS-ReID, respectively. Such results show our SeCap can effectively mitigate view bias in the AGPReID task.

Compared to cross-view competitors, our method also exhibits better performance. It is because we adaptively recalibrate prompts to match the current view based on the view-invariant information, significantly enhancing cross-

Table 5. The efficacy of components in SeCap is evaluated on the LAGPeR and G2APS-ReID datasets. 'Baseline' represents the ReID method utilizing ViT as the backbone, 'LFRM' denotes the Local Feature Refinement Module, 'VDT' refers to the View Decoupling Transformer, and 'PRM' means the Prompt Re-calibration Module. The best performance and best improvements are in **bold**.

NO.	METHOD	LAGPeR						G2APS-ReID			
		$A \to G$		$G \to A$		$G \to A + G$		$A \to G$		$G \to A$	
		Rank-1	mAP	Rank-1	mAP	Rank-1	mAP	Rank-1	mAP	Rank-1	mAP
1	Baseline (ViT)	38.67	27.25	32.04	30.69	18.88	15.31	69.38	52.17	67.16	52.22
2	+ VDT	40.15	28.97	33.55	31.98	19.50	16.45	73.05	56.23	71.08	56.01
		+1.48	+1.72	+1.51	+1.29	+0.62	+1.14	+3.67	+4.06	+3.92	+3.79
3	+ LFRM	40.05	28.76	33.85	32.10	22.23	18.45	72.74	56.06	70.47	56.60
		+1.38	+1.51	+1.81	+1.41	+3.35	+3.14	+3.36	+3.89	+3.31	+4.38
4	+ LFRM + PRM	39.36	28.52	33.06	31.46	22.13	17.47	72.72	55.89	69.79	56.18
		+0.69	+1.27	+1.02	+0.77	+3.25	+2.16	+3.34	+3.72	+2.63	+3.96
5	+ LFRM + VDT	41.56	30.15	34.96	33.38	23.57	18.96	73.58	57.42	72.31	58.02
		+2.89	+2.90	+2.92	+2.69	+4.69	+3.65	+4.20	+5.25	+5.15	+5.80
6	+ LFRM + VDT + PRM (*Ours*)	**41.79**	**30.37**	**35.26**	**33.42**	**24.39**	**19.24**	**75.31**	**58.57**	**73.22**	**58.90**
		+3.12	**+3.12**	**+3.22**	**+2.73**	**+5.51**	**+3.93**	**+5.93**	**+6.40**	**+6.06**	**+6.68**

view person re-identification performance.

5.3. Ablation Study

To systematically evaluate the contributions of each module in our proposed SeCap method, we design and conduct a series of ablation experiments, as shown in Tab. 5. (1) The experimental results indicate that the **LFRM can significantly enhance model performance** by refining local features (#1 vs.#3). (2) The VDT leverages its viewpoint decoupling capabilities to **partially eliminate the interference of viewpoint factors on feature representations** (#1 vs.#2). However, after adding the LFRM, **the performance of the model is further improved** (#2 vs.#5). (3) Although the results of #4 show some improvement compared to the baseline, it is **no better than using the LFRM alone** (#3 vs.#4). However, **the model performs best when the PRM is added to #5**. This is because the PRM relies on the view-invariant features decoupled by the VDT to recalibrate the prompts. Without VDT, the prompts learn incorrect view-invariant information, leading to performance degradation. **Conversely, decoupling the features allows the PRM to fully leverage the correct view-invariant information, achieving the best performance.**

5.4. Feature visualization

As shown in Fig. 3, we visualize the cross-view person identity features extracted by SeCap from the LAGPeR dataset. The results demonstrate that, compared with the baseline model, our proposed SeCap exhibits stronger intra-class cohesion and inter-class discrimination. Additionally, it can effectively extract discriminative cross-view features from images with the same ID under different views.

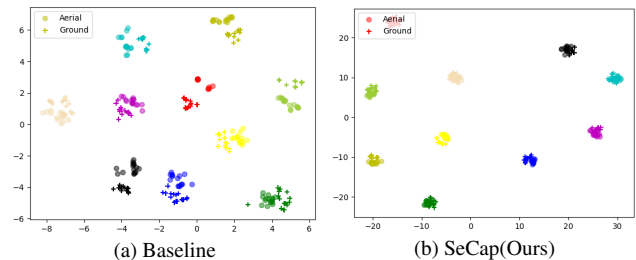(a) Baseline   (b) SeCap(Ours)

Figure 3. Visualize the features extracted by SeCap and the baseline model using t-SNE. Circles (●) represent the Aerial View, and pluses (+) represent the Ground View. The same IDs are indicated by the same color.

6. Conclusion

This paper focuses on cross-view ReID, specifically AG-PReID. Firstly, we propose the Self-Calibrating and Adaptive Prompts (SeCap) method to address the significant view differences. By re-calibrate prompts to match the current view based on the input adaptively, the SeCap significantly enhances model performance. Secondly, we contribute two real-world large-scale AGPReID datasets, LAGPeR and G2APS-ReID. Finally, the experiments on AG-PReID datasets demonstrate the superiority of our method.

References

[1] Leyde Briceno and Gunther Paul. Makehuman: a review of the modelling framework. In *Proceedings of the 20th Congress of the International Ergonomics Association (IEA 2018) Volume V: Human Simulation and Virtual Environments, Work With Computing Systems (WWCS), Process Control 20*, pages 224–232. Springer, 2019. 2

[2] Nicolas Carion, Francisco Massa, Gabriel Synnaeve, Nicolas Usunier, Alexander Kirillov, and Sergey Zagoruyko. End-to-end object detection with transformers. In *European conference on computer vision*, pages 213–229. Springer, 2020. 4

[3] Qi Chen, Yun Chen, Yuheng Huang, Xiaohua Xie, and Lingxiao Yang. Region-based online selective examination for weakly supervised semantic segmentation. *Information Fusion*, 107:102311, 2024. 3

[4] Shuoyi Chen, Mang Ye, and Bo Du. Rotation invariant transformer for recognizing object in uavs. In *Proceedings of the 30th ACM International Conference on Multimedia*, pages 2565–2574, 2022. 1, 3

[5] Jia Deng, Wei Dong, Richard Socher, Li-Jia Li, Kai Li, and Li Fei-Fei. Imagenet: A large-scale hierarchical image database. In *2009 IEEE conference on computer vision and pattern recognition*, pages 248–255. Ieee, 2009. 6

[6] Lingxiao He, Xingyu Liao, Wu Liu, Xinchen Liu, Peng Cheng, and Tao Mei. FastReID: A Pytorch Toolbox for General Instance Re-identification. In *Proceedings of the 31st ACM International Conference on Multimedia*, pages 9664–9667, Ottawa ON Canada, 2023. ACM. 2

[7] Shuting He, Hao Luo, Pichao Wang, Fan Wang, Hao Li, and Wei Jiang. Transreid: Transformer-based object re-identification. In *Proceedings of the IEEE/CVF international conference on computer vision*, pages 15013–15022, 2021. 2, 3, 7

[8] Weizhen He, Yiheng Deng, Shixiang Tang, Qihao Chen, Qingsong Xie, Yizhou Wang, Lei Bai, Feng Zhu, Rui Zhao, Wanli Ouyang, et al. Instruct-reid: A multi-purpose person re-identification task with instructions. In *Proceedings of the IEEE/CVF Conference on Computer Vision and Pattern Recognition*, pages 17521–17531, 2024. 3

[9] Yan Huang, Qiang Wu, Zhang Zhang, Caifeng Shan, Yi Zhong, and Liang Wang. Meta clothing status calibration for long-term person re-identification. *IEEE Transactions on Image Processing*, 2024. 3

[10] Khadija Khaldi, Vuong D Nguyen, Pranav Mantini, and Shishir Shah. Unsupervised person re-identification in aerial imagery. In *Proceedings of the IEEE/CVF Winter Conference on Applications of Computer Vision*, pages 260–269, 2024. 1

[11] Geon Lee, Sanghoon Lee, Dohyung Kim, Younghoon Shin, Yongsang Yoon, and Bumsub Ham. Camera-driven representation learning for unsupervised domain adaptive person re-identification. In *Proceedings of the IEEE/CVF International Conference on Computer Vision*, pages 11453–11462, 2023. 1

[12] He Li, Mang Ye, and Bo Du. Weperson: Learning a generalized re-identification model from all-weather virtual data. In *Proceedings of the 29th ACM international conference on multimedia*, pages 3115–3123, 2021. 1

[13] Siyuan Li, Li Sun, and Qingli Li. Clip-reid: exploiting vision-language model for image re-identification without concrete text labels. In *Proceedings of the AAAI Conference on Artificial Intelligence*, pages 1405–1413, 2023. 3, 7

[14] Tianjiao Li, Jun Liu, Wei Zhang, Yun Ni, Wenqian Wang, and Zhiheng Li. Uav-human: A large benchmark for human behavior understanding with unmanned aerial vehicles. In *Proceedings of the IEEE/CVF conference on computer vision and pattern recognition*, pages 16266–16275, 2021. 1, 2, 3

[15] Fan Liu, Liang Yao, Chuanyi Zhang, Ting Wu, Xinlei Zhang, Xiruo Jiang, and Jun Zhou. Scale-Invariant Feature Disentanglement via Adversarial Learning for UAV-based Object Detection, 2024. arXiv:2405.15465 [cs]. 2

[16] Ze Liu, Yutong Lin, Yue Cao, Han Hu, Yixuan Wei, Zheng Zhang, Stephen Lin, and Baining Guo. Swin transformer: Hierarchical vision transformer using shifted windows. In *Proceedings of the IEEE/CVF international conference on computer vision*, pages 10012–10022, 2021. 2, 3, 6, 7

[17] Hao Luo, Youzhi Gu, Xingyu Liao, Shenqi Lai, and Wei Jiang. Bag of tricks and a strong baseline for deep person re-identification. In *Proceedings of the IEEE/CVF conference on computer vision and pattern recognition workshops*, pages 0–0, 2019. 7, 2, 3

[18] Jiaxu Miao, Yu Wu, Ping Liu, Yuhang Ding, and Yi Yang. Pose-Guided Feature Alignment for Occluded Person Re-Identification. In *2019 IEEE/CVF International Conference on Computer Vision (ICCV)*, pages 542–551, Seoul, Korea (South), 2019. IEEE. 2

[19] Grégoire Montavon, Geneviève Orr, and Klaus-Robert Müller. *Neural networks: tricks of the trade*. springer, 2012. 7

[20] Huy Nguyen, Kien Nguyen, Sridha Sridharan, and Clinton Fookes. Aerial-ground person re-id. In *2023 IEEE International Conference on Multimedia and Expo (ICME)*, pages 2585–2590. IEEE, 2023. 1, 2, 3, 6, 7

[21] Huy Nguyen, Kien Nguyen, Sridha Sridharan, and Clinton Fookes. Ag-reid. v2: Bridging aerial and ground views for person re-identification. *IEEE Transactions on Information Forensics and Security*, 2024. 1, 2, 3, 6

[22] Enhao Ning, Yangfan Wang, Changshuo Wang, Huang Zhang, and Xin Ning. Enhancement, integration, expansion: Activating representation of detailed features for occluded person re-identification. *Neural Networks*, 169:532–541, 2024. 2

[23] Xuelin Qian, Yanwei Fu, Tao Xiang, Wenxuan Wang, Jie Qiu, Yang Wu, Yu-Gang Jiang, and Xiangyang Xue. Pose-normalized image generation for person re-identification. In *Proceedings of the European conference on computer vision (ECCV)*, pages 650–667, 2018. 1

[24] Xuelin Qian, Yanwei Fu, Tao Xiang, Yu-Gang Jiang, and Xiangyang Xue. Leader-based multi-scale attention deep architecture for person re-identification. *IEEE transactions on pattern analysis and machine intelligence*, 42(2):371–385, 2019. 1

[25] Xuelin Qian, Wenxuan Wang, Li Zhang, Fangrui Zhu, Yanwei Fu, Tao Xiang, Yu-Gang Jiang, and Xiangyang Xue. Long-term cloth-changing person re-identification. In *Proceedings of the Asian conference on computer vision*, 2020. 1

[26] Yang Qin, Yingke Chen, Dezhong Peng, Xi Peng, Joey Tianyi Zhou, and Peng Hu. Noisy-correspondence learning for text-to-image person re-identification. In *Proceedings of the IEEE/CVF Conference on Computer Vision and Pattern Recognition*, pages 27197–27206, 2024. 3

[27] Yifan Sun, Liang Zheng, Yi Yang, Qi Tian, and Shengjin Wang. Beyond part models: Person retrieval with refined part pooling (and a strong convolutional baseline). In *Proceedings of the European conference on computer vision (ECCV)*, pages 480–496, 2018. 1, 2

[28] Lei Wang, Quan Zhang, Junyang Qiu, and Jianhuang Lai. Rotation exploration transformer for aerial person re-identification. In *2024 IEEE International Conference on Multimedia and Expo (ICME)*, pages 1–6. IEEE, 2024. 1

[29] Qizao Wang, Xuelin Qian, Bin Li, Xiangyang Xue, and Yanwei Fu. Exploring fine-grained representation and recomposition for cloth-changing person re-identification. *IEEE Transactions on Information Forensics and Security*, 2024. 1

[30] Longhui Wei, Shiliang Zhang, Wen Gao, and Qi Tian. Person transfer gan to bridge domain gap for person re-identification. In *Proceedings of the IEEE conference on computer vision and pattern recognition*, pages 79–88, 2018. 3

[31] Ruiqi Wu, Bingliang Jiao, Wenxuan Wang, Meng Liu, and Peng Wang. Enhancing visible-infrared person re-identification with modality-and instance-aware visual prompt learning. In *Proceedings of the 2024 International Conference on Multimedia Retrieval*, pages 579–588, 2024. 3, 7

[32] Cheng Yan, Guansong Pang, Lei Wang, Jile Jiao, Xuetao Feng, Chunhua Shen, and Jingjing Li. BV-Person: A Large-scale Dataset for Bird-view Person Re-identification. In *2021 IEEE/CVF International Conference on Computer Vision (ICCV)*, pages 10923–10932, Montreal, QC, Canada, 2021. IEEE. 2

[33] Mouxing Yang, Zhenyu Huang, and Xi Peng. Robust object re-identification with coupled noisy labels. *International Journal of Computer Vision*, pages 1–19, 2024. 3

[34] Mang Ye, Jianbing Shen, Gaojie Lin, Tao Xiang, Ling Shao, and Steven CH Hoi. Deep learning for person re-identification: A survey and outlook. *IEEE transactions on pattern analysis and machine intelligence*, 44(6):2872–2893, 2021. 1, 7, 2

[35] Pingping Zhang, Yuhao Wang, Yang Liu, Zhengzheng Tu, and Huchuan Lu. Magic Tokens: Select Diverse Tokens for Multi-modal Object Re-Identification, 2024. arXiv:2403.10254 [cs].

[36] Quan Zhang, Jianhuang Lai, Zhanxiang Feng, and Xiaohua Xie. Uncertainty modeling for group re-identification. *International Journal of Computer Vision*, pages 1–21, 2024. 1

[37] Quan Zhang, Jianhuang Lai, Xiaohua Xie, Xiaofeng Jin, and Sien Huang. Separable spatial-temporal residual graph for cloth-changing group re-identification. *IEEE Transactions on Pattern Analysis and Machine Intelligence*, 2024. 1

[38] Quan Zhang, Lei Wang, Vishal M Patel, Xiaohua Xie, and Jianhaung Lai. View-decoupled transformer for person re-identification under aerial-ground camera network. In *Proceedings of the IEEE/CVF Conference on Computer Vision and Pattern Recognition*, pages 22000–22009, 2024. 1, 2, 3, 6, 7

[39] Shizhou Zhang, Qi Zhang, Yifei Yang, Xing Wei, Peng Wang, Bingliang Jiao, and Yanning Zhang. Person re-identification in aerial imagery. *IEEE Transactions on Multimedia*, 23:281–291, 2020. 1, 2, 3

[40] Shizhou Zhang, Qingchun Yang, De Cheng, Yinghui Xing, Guoqiang Liang, Peng Wang, and Yanning Zhang. Ground-to-aerial person search: Benchmark dataset and approach. In *Proceedings of the 31st ACM International Conference on Multimedia*, pages 789–799, 2023. 2, 5, 6

[41] Xuan Zhang, Hao Luo, Xing Fan, Weilai Xiang, Yixiao Sun, Qiqi Xiao, Wei Jiang, Chi Zhang, and Jian Sun. AlignedReID: Surpassing Human-Level Performance in Person Re-Identification, 2018. arXiv:1711.08184 [cs]. 1

[42] Liang Zheng, Liyue Shen, Lu Tian, Shengjin Wang, Jiahao Bu, and Qi Tian. Person re-identification meets image search. *arXiv preprint arXiv:1502.02171*, 2015. 2, 3

[43] Zhedong Zheng, Liang Zheng, and Yi Yang. Unlabeled samples generated by gan improve the person re-identification baseline in vitro. In *Proceedings of the IEEE international conference on computer vision*, pages 3754–3762, 2017. 2, 3

SeCap: Self-Calibrating and Adaptive Prompts for Cross-view Person Re-Identification in Aerial-Ground Networks

Supplementary Material

7. Overview

In this supplementary material, we provide additional experimental results and more in-depth discussions of the following three aspects:

- We conduct a visual analysis comparing our proposed SeCap method with the baseline model, including retrieval results and attention map.
- We perform experiments on the AGPReID datasets GARGO [38] and AG-ReID.v2 [21], demonstrating that SeCap is a feasible and effective solution for the AGPReID task across all publicly available AGPReID datasets. Additionally, we conducted cross-dataset evaluation experiments.
- We analyze the impact of prompt length L and hyperparameter λ on model performance and conduct ablation experiments on the individual modules to verify the effectiveness of our method.

Unless otherwise specified, the numbering of figures and tables should be within the scope of the supplementary material, and consistent with the main paper.

8. Visual Analysis

8.1. Retrieval Result Visualization

The visualization of the retrieval results compellingly demonstrates that SeCap is a feasible and effective method for addressing the challenges posed by AG-PReID problems. As illustrated in Fig. 4, the retrieval outcomes on both LAGPeR and AG-ReID datasets are presented, offering a comprehensive comparison of SeCap's retrieval results with those of baseline methods across various experimental settings.

8.2. Attention Map Visualization

We visualized the attention maps of some case images from both the SeCap method and the baseline model. As shown in Fig. 5, the baseline model tends to focus more on the torso or clothing of individuals rather than view-invariant regions like head features. **In contrast, our SeCap method effectively attends to view-invariant local features, ensuring robust performance across varying viewpoints.**

9. Performance on Other AGPReID Datasets

9.1. Dataset.

(1) AG-ReID.v2: This dataset comprises $100,502$ images with $1,605$ unique IDs, captured by three types of cameras:
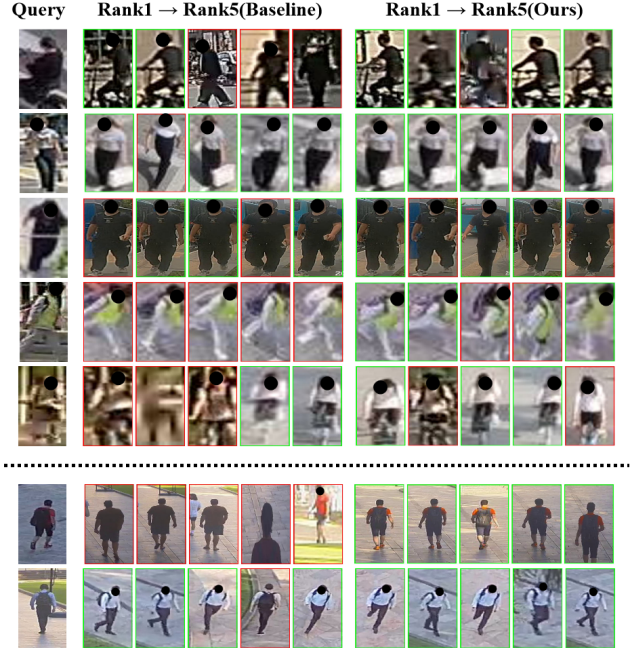

Figure 4. Comparison of several retrieval visualizations on the LAGPeR dataset of setting $A \rightarrow G$. Red and green boxes represent wrong and correct matchings. The top five are listed.
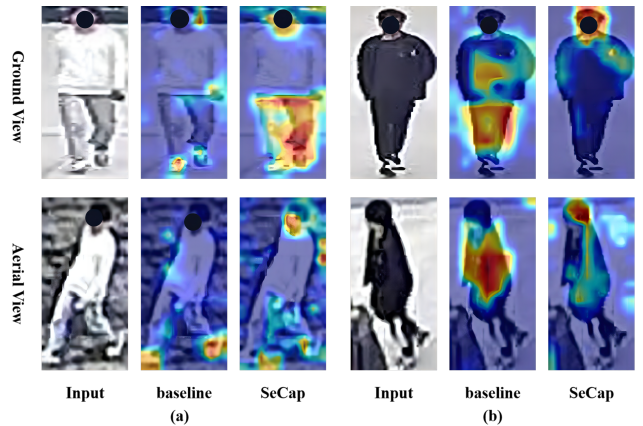

Figure 5. The visualization results of the attention maps of our SeCap method and the baseline model.

CCTV, UAV, and wearable devices [21]. Among these, 807 IDs are designated for the training set, while the remaining 798 IDs are used for the test set. Additionally, the dataset includes 15 attributes to facilitate cross-view matching. In terms of experimental settings, the test images are evaluated

Table 6. Performance comparison under CARGO dataset. 'ALL' denotes the overall retrieval performance of each method. '$G \leftrightarrow G$', '$A \leftrightarrow A$', and '$A \leftrightarrow G$' represent the performance of each model in several specific retrieval patterns.Rank1 and mAP are reported (%). The best performance is shown in **bold**.

METHOD	BACKBONE	ALL		$G \leftrightarrow G$		$A \leftrightarrow A$		$A \leftrightarrow G$	
		Rank-1	mAP	Rank-1	mAP	Rank-1	mAP	Rank-1	mAP
SBS [6]	R50	50.32	43.09	72.31	62.99	67.50	49.73	31.25	29.00
AGW [34]	R50	60.26	53.44	81.25	71.66	67.50	56.48	43.57	40.90
BoT [17]	ViT	61.54	53.54	82.14	71.34	80.00	64.47	43.13	40.11
VDT [38]	ViT	64.10	55.2	82.14	71.59	**82.50**	66.83	48.12	42.76
SeCap(Ours)	ViT	**68.59**	**60.19**	**86.61**	**75.42**	80.00	**68.08**	**69.43**	**58.94**

Table 7. Performance comparison on the AG-ReID.v2 dataset. C represents CCTV, W represents wearable devices, and A represents aerial views. The best results are highlighted in **bold**, while the second-best results are <u>underlined</u>.

METHOD	BACKBONE	$A \rightarrow C$		$C \rightarrow A$		$A \rightarrow W$		$W \rightarrow A$	
		Rank-1	mAP	Rank-1	mAP	Rank-1	mAP	Rank-1	mAP
BoT [17]	ViT	85.40	77.03	84.65	75.90	89.77	80.48	84.65	75.90
AG-ReIDv1 [20]	ViT	87.70	79.00	87.35	78.24	**93.67**	83.14	<u>87.73</u>	79.08
VDT [38]	ViT	86.46	79.13	86.14	78.12	90.00	82.21	85.26	78.52
AG-ReIDv2 [21]	ViT	**88.77**	<u>80.72</u>	<u>87.86</u>	<u>78.51</u>	93.62	**84.85**	**88.61**	<u>80.11</u>
SeCap(Ours)	ViT	<u>88.12</u>	**80.84**	**88.24**	**79.99**	91.44	<u>84.01</u>	87.56	**80.15**

under the following conditions: $A \rightarrow C$, $C \rightarrow A$, $A \rightarrow W$, and $W \rightarrow A$.

(2) CARGO: The CARGO dataset is a virtual AGPReID dataset constructed using tools such as MakeHuman [1] and Unity3D. It comprises $108,563$ images with $5,000$ unique IDs, captured by 13 cameras: 8 ground cameras and 5 aerial cameras. Among these, $51,451$ images from $2,500$ IDs are designated for the training set, while the remaining $51,024$ images from $2,500$ IDs are used for the test set. In terms of experimental settings, the test images are evaluated under four conditions: ALL, $A \leftrightarrow A$, $G \leftrightarrow G$, and $A \leftrightarrow G$. The "ALL" setting focuses on comprehensive retrieval performance, while the latter targets specific retrieval scenarios.

9.2. Performance.

On additional AGPReID datasets, SeCap demonstrates robust performance. Tab. 7 and Tab. 6 present the performance of the proposed SeCap on the AG-ReID.v2 [21] and CARGO [38] datasets. It can be seen that **SeCap achieves optimal results across various settings on the synthetic AGPReID dataset CARGO and significantly outperforms other methods in the cross-view task $A \leftrightarrow G$, demonstrating the significant advantages of our pro-**

posed method in solving cross-view problems. In the setting $A \leftrightarrow A$, due to the limited number of queries in CARGO, which consists of only 60 IDs with 134 images, the chance level is 2.5%. Consequently, the Rank1 performance is relatively close. However, when considering the metric of mAP metric, which better reflects the model's performance, our method demonstrates superior results.

On the AG-ReID.v2 dataset, we compare AGPReID methods such as AG-ReID.v1, VDT, and AG-ReID.v2. AG-ReID.v1 only reports results using ResNet-50 as the backbone on the AG-ReID.v2 dataset, so we compare the results of ViT enhanced by the Explainable ReID Stream(EP). As shown in Tab. 7, we observe that **even without using the attributes provided by AG-ReID.v2, our method still achieved the best or comparable results in the $A \rightarrow C$ and $C \rightarrow A$ experimental settings. In the $A \rightarrow W$ and $W \rightarrow A$ settings, our method achieves the best or comparable mAP results, but its Rank-1 metric is not as high as AG-ReID.v2.** This discrepancy arises because our SeCap method uses view-invariant local features for matching, with head information being a significant view-invariant feature. From Fig. 5, it is evident that our method implicitly trains the model to

Table 8. The analysis of the effectiveness of the PRM and LFRM in SeCap. LFRM stands for the Local Feature Refinement Module, PRM denotes the Prompt Re-calibration Module, and OLP represents Overlapping Patches. The meanings of Add, Cat, and Attn are detailed in the Sec. 11. The best performance and the most significant improvements are highlighted in **bold**.

No.	PRM			LFRM			OLP	$A \to G$		$G \to A$		$G \to A + G$	
	Add	Cat	Attn.	Block	Two-Way	fusion		Rank-1	mAP	Rank-1	mAP	Rank-1	mAP
1	✔				✔	✔	✔	38.48	27.76	32.14	30.49	22.75	18.49
2		✔			✔	✔	✔	40.09	29.10	33.88	32.71	22.52	18.44
3			✔	✔		✔	✔	39.92	28.59	33.32	31.55	22.88	18.60
4			✔		✔		✔	40.25	28.88	34.11	32.25	21.14	17.23
5			✔		✔	✔		40.87	29.11	33.72	32.48	19.67	16.40
6			✔		✔	✔	✔	**41.8**	**30.4**	**35.3**	**33.4**	**24.39**	**19.24**

focus more on head features. Conversely, AG-ReID.v2's Elevated-View Attention Stream(EVA) explicitly uses head information for cross-view matching, which is generally more robust than implicitly extracting local features, resulting in better Rank-1 performance. However, this approach may fail when the head is occluded, leading to a significant performance drop. Therefore, our method performs better on the average mAP metric, which better indicates the model's re-identification capability [42]. Additionally, in the $A \to W$ setting, we found that the improvement in model performance is mainly due to the attribute-based Explainable ReID Stream(EP), rather than the Elevated-View Attention Stream (EVA), which has the limitation of relying on attribute labels.

10. Cross-dataset evaluation

The proposed SeCap method in this study demonstrates superiority over other methods in cross-dataset evaluation. Specifically, as shown in Tab. 9, the results of training on the LAGPeR dataset and testing on the AR-ReID dataset indicate that direct cross-dataset (or cross-domain) evaluation is a challenging task. However, the SeCap method exhibits more significant advantages compared to baseline methods and the VDT method. This advantage may stem from the dynamically generated and calibrated prompt mechanism of SeCap, which not only learns perspective-irrelevant features but also effectively guides the model to focus more on cross-domain identity discrimination features, thereby promoting the model to learn more discriminative feature representations.

11. Effectiveness Analysis of the Modules

As shown in Tab. 8, we analyze the roles of the Prompt Re-calibration Module (**PRM**), Local Feature Refinement Module (**LFRM**), and Overlapping Patches(**OLP**).

Table 9. Cross-dataset performance evaluations (%) for transferring from LAGPeR to AG-ReID dataset.

METHOD	BB	$A \to G$		$G \to A$	
		Rank-1	mAP	Rank-1	mAP
BoT [17]	ViT	33.15	22.7	28.90	20.32
VDT [38]	ViT	34.74	23.42	29.83	21.53
SeCap(Ours)	ViT	**37.93**	**24.96**	**30.87**	**22.99**

For the Prompt Re-calibration Module(PRM), we explore different methods of incorporating view-invariant features by comparing the Add, Cat, and Attn methods (#1 vs #2 vs #6). Add represents the method of integrating view-invariant features into the prompts through addition; Cat involves concatenating view-invariant features to the prompts and integrating them via self-attention; Attn involves learning view-invariant information through the attention mechanism, which is the method used in **PRM**. Among these methods, Attn achieves the best results.
For the LFRM module, we compare the effects of using two-way attention and Transformer decoding blocks (#3 vs #6). The two decoding structures are shown in Fig. 8, where the two-way attention(Two-Way) demonstrate significant performance improvements. Additionally, we validate the effectiveness of the feature fusion module (#4 vs #6), confirming its utility. Lastly, we assess the impact of overlapping patches (#5 vs #6), which also contribute to performance enhancement.

12. Parameter Analysis

As illustrated in Fig. 6, we analyze the impact of the hyperparameter λ on the model's performance. When λ is set to
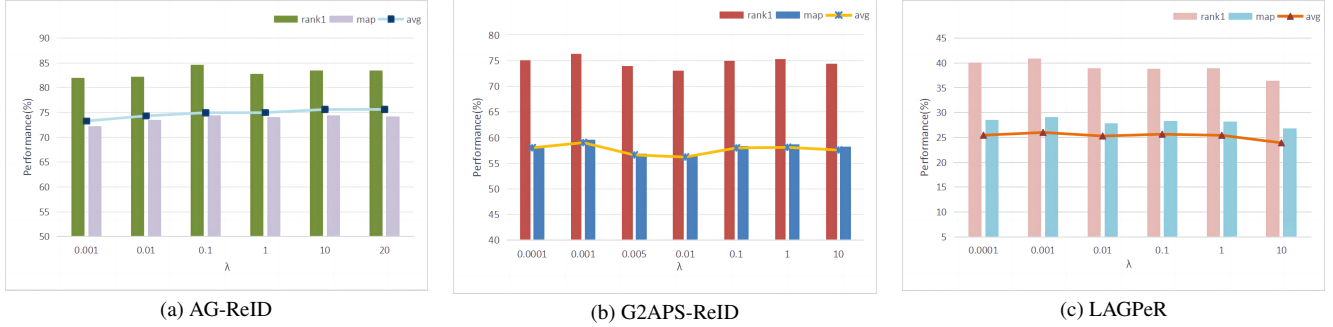
Figure 6. Fig. 6a ~ Fig. 6c show the impact of hyperparameter λ on model performance under three datasets. For simplicity, only setting $A \rightarrow G$ is shown on the AGPReID datasets. Rank1 and mAP are reported (%). The avg represents the average performance of mAP.
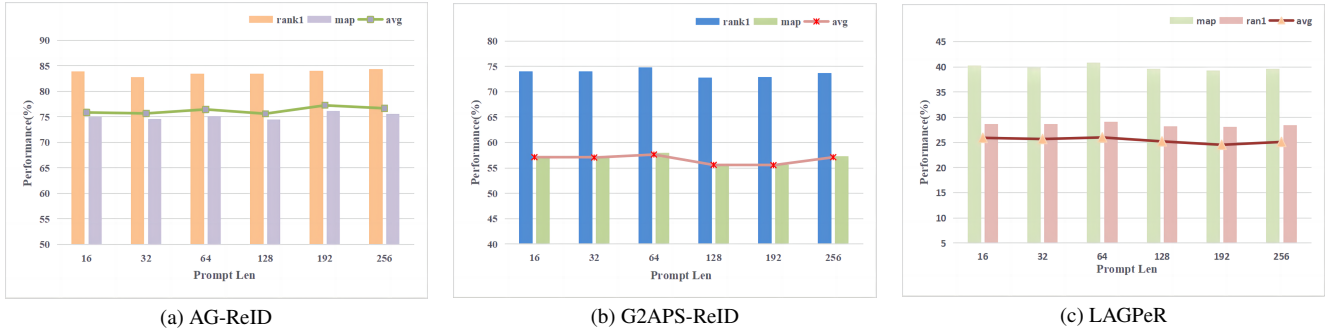

Figure 7. Fig. 7a ~ Fig. 7c show the impact of prompt length L on model performance under three datasets. For simplicity, only setting $A \rightarrow G$ is shown on the AGPReID datasets. Rank1 and mAP are reported (%). The avg represents the average performance of mAP.

0.001, the SeCap model performs best on the G2APS-ReID and LAGPeR datasets. For the AG-ReID dataset, the optimal λ is 10. **This discrepancy arises because the G2APS-ReID and LAGPeR datasets have a higher number of IDs, necessitating a smaller coefficient to balance the difficulty between viewpoint classification and ID classification.**

Under the identical λ setting, we carry out a detailed analysis of the impact of prompt length L on the model's performance. As presented in Fig. 7, **the model's performance is not highly sensitive to the prompt length L.** The model attains the best performance when the prompt length is set to 64.

13. Broader impact

The proposed method can be applied to existing aerial-ground person re-identification tasks, aiming to improve the performance of AGPReID tasks. All experiments are based on publicly available datasets, reconstructed datasets from public datasets, and datasets from public datasets, with the core goal of optimizing the application effect of the recognition model in real-world scenarios, rather than deliberately designing privacy leakage mechanisms. However, it is necessary to be vigilant against potential negative effects,

such as the privacy leakage risks that may arise from using surveillance and drone-captured person re-identification data. Therefore, when collecting such data, we ensure that relevant individuals are fully informed and strictly manage and use the data to protect individuals' privacy rights and interests.
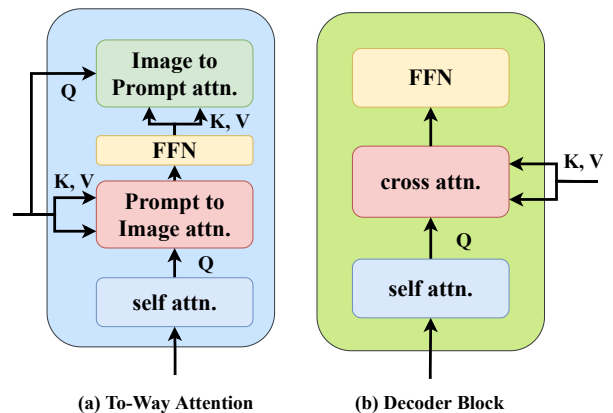

Figure 8. The structure of Two-Way attention and Transformer Decoding Block.

14. Scene examples of the LAGPeR dataset.

As Fig.9, we show some scene examples of the LAGPeR dataset, where A-Cam represents the aerial view camera and G-Cam represents the ground view camera. Each column represents the same scene.
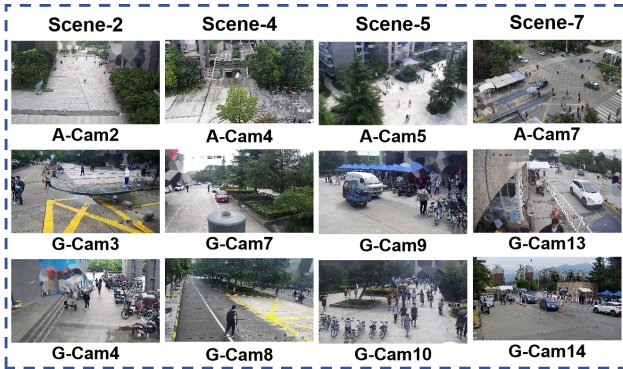

Figure 9. Example images from the LAGPeR, where each column represents images from the same scene.

15. Performance of $G \leftrightarrow G$

Our method achieves better results than top-performing compared methods in the $G \leftrightarrow G$ setting. We reconstructed the LAGPeR dataset and created the $G \leftrightarrow G$ subset to evaluate our model's performance, and the results are presented in Tab.10.

Table 10. Performance comparison on the $G \leftrightarrow G$ setting.

METHOD	ViT	VDT	TransReID	SeCap
Rank-1	78.36	77.18	79.23	**79.57**
mAP	77.38	76.35	78.09	**78.26**